

A NEW VERSION OF THE ADAPTIVE FAST GAUSS TRANSFORM FOR DISCRETE AND CONTINUOUS SOURCES

LESLIE GREENGARD*, SHIDONG JIANG†, MANAS RACHH‡, AND JUN WANG§

Abstract. We present a new version of the fast Gauss transform (FGT) for discrete and continuous sources. Classical Hermite expansions are avoided entirely, making use only of the plane-wave representation of the Gaussian kernel and a new hierarchical merging scheme. For continuous source distributions sampled on adaptive tensor-product grids, we exploit the separable structure of the Gaussian kernel to accelerate the computation. For discrete sources, the scheme relies on the nonuniform fast Fourier transform (NUFFT) to construct near field plane wave representations. The scheme has been implemented for either free-space or periodic boundary conditions. In many regimes, the speed is comparable to or better than that of the conventional FFT *in work per gridpoint*, despite being fully adaptive.

Key words. fast Gauss transform, Fourier spectral approximation, nonuniform fast Fourier transform, level-restricted adaptive tree.

AMS subject classifications. 31A10, 65F30, 65E05, 65Y20

1. Introduction. In this paper, we consider the evaluation of the discrete and continuous Gauss transforms:

$$(1.1) \quad u_i = \sum_{j=1}^N G(\mathbf{x}_i - \mathbf{y}_j; \delta) q_j, \quad \mathbf{x}_i, \mathbf{y}_j \in B, \quad i = 1, \dots, M,$$

and

$$(1.2) \quad u(\mathbf{x}) = \int_B G(\mathbf{x} - \mathbf{y}; \delta) \sigma(\mathbf{y}) d\mathbf{y},$$

where $B = [-\frac{1}{2}, \frac{1}{2}]^d$ is the unit box centered at the origin in \mathbb{R}^d . For free space problems, the Gaussian kernel is given by

$$(1.3) \quad G(\mathbf{x}; \delta) = e^{-\frac{\|\mathbf{x}\|^2}{\delta}},$$

while for periodic problems,

$$(1.4) \quad G(\mathbf{x}; \delta) = \sum_{\mathbf{j} \in \mathbb{Z}^d} e^{-\frac{\|\mathbf{x} + \mathbf{j}\|^2}{\delta}},$$

where \mathbb{Z}^d denotes the d -dimensional integer lattice. This task is ubiquitous in computational physics, engineering, and statistics and we do not seek to review the various applications here.

*Center for Computational Mathematics, Flatiron Institute, Simons Foundation, New York, New York 10010 & Courant Institute of Mathematical Sciences, New York University, New York, New York 10012 (greenard@courant.nyu.edu).

†Center for Computational Mathematics, Flatiron Institute, Simons Foundation, New York, New York 10010 (sjiang@flatironinstitute.org).

‡Center for Computational Mathematics, Flatiron Institute, Simons Foundation, New York, New York 10010 (mrachh@flatironinstitute.org).

§Yau Mathematical Sciences Center, Tsinghua University, Beijing China 100084 (jwang2020@tsinghua.edu.cn).

The original fast Gauss transform (FGT) [10] is a single level scheme that superimposes on B a uniform grid of boxes of side length $O(\sqrt{\delta})$ - ensuring that interactions are negligible outside a modest range of near neighbors. More concretely, if the uniform grid spacing is exactly $\sqrt{\delta}$, then after four neighbors in any direction, the Gaussian has decayed to approximately 10^{-7} and an expansion of the field induced by the Gaussians in terms of Hermite functions requires an expansion of about 10^d terms to achieve seven digit accuracy within the region of interest. Using this “low-rank representation”, the FGT is a linear scaling algorithm, requiring only $O(M + N)$ work for the evaluation of (1.1).

REMARK 1.1. *Reducing the number of boxes within the region of interest can be accomplished by setting the box size to $4\sqrt{\delta}$, so that only near neighbors need be considered. However, the necessary expansion size then increases to more than 40^d , and the algorithm is less efficient.*

Since the creation of the original FGT, several improvements and extensions have been made (see, for example, [7, 11, 13, 16, 17, 18, 20, 23, 24]). Of particular relevance are [11, 16, 17], where Fourier-based methods were introduced, providing efficient approximations which can be translated in diagonal form - yielding significant accelerations. Also relevant is [24], which uses both Hermite and Fourier-based expansions. It is hierarchical, fully adaptive, insensitive to δ , and able to compute transforms with discrete sources, volume sources and densities supported on boundaries. The algorithmic approach in [24] follows that of the hierarchical fast multipole method (FMM) [9], separating near and far field interactions.

Here, we introduce an alternate scheme, which turns out to be both simpler and faster. The new scheme eliminates the Hermite and local expansions that have been central to previous FGTs. Instead, it relies only on the Fourier (spectral) approximation of the Gaussian. For discrete sources, given a parameter s , an adaptive tree is constructed by hierarchically dividing every box containing more than s particles into 2^d child boxes, until it reaches the so-called “cutoff” level l_c with box dimension approximately $\sqrt{\log(\frac{3}{\epsilon})} \sqrt{\delta}$ (discussed in section 3). Briefly, the cutoff level is chosen so that only interactions between neighboring boxes need to be considered for computing the potential to the specified accuracy ϵ .

The interactions between boxes at the cutoff level which contain more than s sources and targets are handled using plane-wave expansions. This representation is particularly efficient, since translation is diagonal in the plane wave basis (as they are eigenfunctions of the translation operator). Since one only needs to consider the interactions between nearest neighbors, the number of diagonal translations is minimal, especially when compared with the FMM-like FGT in [24].

A key observation used in the new scheme is that the formation and evaluation of these plane-wave interactions can be accelerated by the nonuniform fast Fourier transforms (NUFFT) [5, 6, 8, 1] at a cost $O(N_F \log N_F + N_P)$, where N_F is the number of discrete Fourier modes and N_P is the number of source and target points. As noted in [2], the prefactor in front of N_P is roughly $(D+1)^d$, where D is the number of requested digits. Thus, the cost of forming and evaluating plane-wave expansions is quite modest in terms of the number of required floating-point operations. The method described in this paper is unusual in that it uses the NUFFT in a spatially adaptive manner. We do *not* use the NUFFT to implement discrete convolution globally, rather to improve the constants in the FGT framework.

For continuous sources, the adaptive tree is designed to resolve the given density

function σ , and thus cannot be terminated at the cutoff level. While one could first apply a quadrature rule to the integral in (1.2) and then call the new point FGT, we can develop a much faster scheme by making use of the tensor product structure of the grid and the separable nature of the Gaussian kernel. To be more precise, integrating a multidimensional Gaussian against a product of polynomials $p_1(x_1) \dots p_d(x_d)$ can be done by building one-dimensional tables of Gaussian convolution integrals for a given δ and a fixed set of target points. Moreover, both forming and evaluating plane-wave expansions can also be accelerated by separation of variables, since the input density is tabulated on a tensor product grid in each leaf box. Detailed analysis of the operation count shows that the diagonal translations needed to merge and split the plane-wave expansions in the adaptive tree hierarchy are negligible contributions to the overall computational cost. The systematic use of the tensor product structure of the continuous FGT (1.2) leads to Algorithm 4.2, below, with single core performance of 5 – 20 million points per second for $d = 2$ and 1 – 7 million points per second for $d = 3$, depending on the precision.

An additional contribution of the present paper is an analysis of the continuous transform (1.2) in terms of *resolution* of the density $\sigma(\mathbf{x})$ and the output potential $u(\mathbf{x})$. While the former may be resolved on the adaptive input grid, it does *not* follow that the latter is resolved on output. In general, it is necessary to build a new adaptive tree that is guaranteed to resolve the potential. We explain the reason for this in subsection 4.3 and describe an algorithm that creates a suitable output tree.

The paper is organized as follows. We begin by reviewing the plane-wave approximation of a Gaussian in section 2. We introduce the new discrete (point) FGT in section 3 and the new continuous (volume) FGT in section 4. Periodic boundary conditions are discussed in section 5. Timing results are presented in section 6 and we conclude in section 7 with a discussion of potential extensions of the present scheme.

2. Mathematical preliminaries. Since the Gaussian in higher dimensions is the product of one-dimensional Gaussians, we need only consider the one-dimensional case in detail. By virtue of the triangle inequality, it is straightforward to see that the error in approximating the Gaussian in \mathbb{R}^d as the product of one-dimensional approximations amplifies the error by a factor of roughly d .

2.1. Spectral approximation of the Gaussian. We will make use of the well-known Fourier transform relation

$$(2.1) \quad G(x; \delta) = e^{-x^2/\delta} = \sqrt{\frac{\delta}{4\pi}} \int_{-\infty}^{\infty} e^{-k^2\delta/4} e^{ikx} dk = \frac{1}{\sqrt{2\pi}} \int_{-\infty}^{\infty} \hat{G}(k; \delta) e^{ikx} dk.$$

Discretizing this integral with the trapezoidal rule yields an approximation of the Gaussian by a finite sum of plane waves [11, 17]. By using the fact that the effective range of x is finite for any specified precision, a modest number of quadrature nodes is sufficient to guarantee uniformly high accuracy. This is made precise in the following lemma.

THEOREM 2.1. *Let $\varepsilon < 0.1$ be a prescribed tolerance, and let us define a “cutoff” length D_0 by the formula*

$$(2.2) \quad D_0 = \sqrt{\log\left(\frac{3}{\varepsilon}\right)}.$$

Then, for any $R \geq D_0$,

$$(2.3) \quad \left| G(x; \delta) - \frac{h}{2\sqrt{\pi}} \sum_{m=-M}^{M-1} e^{-m^2 h^2/4} e^{imhx/\sqrt{\delta}} \right| \leq \varepsilon, \quad |x| \leq R\sqrt{\delta},$$

where M and the stepsize h are given by the formulas

$$(2.4) \quad h = \frac{2\pi}{R + D_0}, \quad M = \left\lceil \frac{2D_0}{h} \right\rceil = \left\lceil \frac{D_0(R + D_0)}{\pi} \right\rceil.$$

Proof. From the Poisson summation formula, it follows that

$$(2.5) \quad \begin{aligned} \sum_{n=-\infty}^{\infty} G\left(x + \frac{2\pi n\sqrt{\delta}}{h}; \delta\right) &= \frac{h}{\sqrt{2\pi\delta}} \sum_{m=-\infty}^{\infty} \hat{G}\left(\frac{mh}{\sqrt{\delta}}\right) e^{imhx/\sqrt{\delta}} \\ &= \frac{h}{2\sqrt{\pi}} \sum_{m=-\infty}^{\infty} e^{-m^2 h^2/4} e^{imhx/\sqrt{\delta}}. \end{aligned}$$

Truncating the right-hand side of (2.5) and rearranging terms, we obtain a Fourier spectral approximation of the Gaussian:

$$(2.6) \quad G(x; \delta) \approx \frac{h}{2\sqrt{\pi}} \sum_{m=-M}^{M-1} e^{-m^2 h^2/4} e^{imhx/\sqrt{\delta}},$$

with error

$$(2.7) \quad \left| G(x; \delta) - \frac{h}{2\sqrt{\pi}} \sum_{m=-M}^{M-1} e^{-m^2 h^2/4} e^{imhx/\sqrt{\delta}} \right| \leq E_T + E_A,$$

where the truncation error E_T is given by

$$(2.8) \quad E_T = \frac{h}{2\sqrt{\pi}} \left| \sum_{m=-\infty}^{-(M+1)} e^{-m^2 h^2/4} e^{imhx/\sqrt{\delta}} + \sum_{m=M}^{\infty} e^{-m^2 h^2/4} e^{imhx/\sqrt{\delta}} \right|,$$

and the ‘‘aliasing’’ error E_A is given by

$$(2.9) \quad E_A = \sum_{\substack{n=-\infty \\ n \neq 0}}^{\infty} G\left(x + \frac{2\pi n\sqrt{\delta}}{h}; \delta\right).$$

For the truncation error, we have

$$(2.10) \quad \begin{aligned} E_T &\leq \frac{h}{\sqrt{\pi}} \sum_{m=M}^{\infty} e^{-m^2 h^2/4} = \frac{h}{\sqrt{\pi}} \sum_{k=0}^{\infty} e^{-(M+k)^2 h^2/4} \\ &= \frac{h}{\sqrt{\pi}} e^{-M^2 h^2/4} \sum_{k=0}^{\infty} e^{-(2kM+k^2)h^2/4} \\ &\leq \frac{h}{\sqrt{\pi}} e^{-M^2 h^2/4} \sum_{k=0}^{\infty} e^{-2kMh^2/4} = \frac{h}{\sqrt{\pi}} \frac{e^{-M^2 h^2/4}}{1 - e^{-2Mh^2/4}}. \end{aligned}$$

For the aliasing error, under the assumption that $|x| \leq R\sqrt{\delta} < 2\pi\sqrt{\delta}/h$, we have

$$\begin{aligned}
 E_A &\leq 2 \sum_{n=1}^{\infty} G\left(\frac{2\pi n\sqrt{\delta}}{h} - R\sqrt{\delta}; \delta\right) \\
 (2.11) \quad &= 2e^{-\left(\frac{2\pi}{h}-R\right)^2} \sum_{k=0}^{\infty} e^{-2\frac{k\pi}{h}\left(\frac{2\pi}{h}-R\right)-\left(\frac{2k\pi}{h}\right)^2} \\
 &\leq \frac{2e^{-\left(\frac{2\pi}{h}-R\right)^2}}{1 - e^{-\frac{4\pi}{h}\left(\frac{2\pi}{h}-R\right)}}.
 \end{aligned}$$

With D_0 given by (2.2), we have

$$(2.12) \quad e^{-D_0^2} \leq \frac{\varepsilon}{3}.$$

By (2.4), we obtain

$$(2.13) \quad e^{-\left(\frac{2\pi}{h}-R\right)^2} = e^{-D_0^2} \leq \varepsilon/3, \quad e^{-M^2 h^2/4} = e^{-D_0^2} \leq \varepsilon/3.$$

From (2.10), (2.11), the assumption that $\varepsilon \leq 0.1$ and the fact that $R \geq D_0$, it is straightforward to verify that

$$(2.14) \quad E_T \leq \varepsilon/3, \quad E_A \leq 2\varepsilon/3.$$

The result (2.3) follows. \square

The total number of quadrature nodes needed in the Fourier spectral approximation, denoted by $n_f(R)$, is simply equal to

$$(2.15) \quad n_f = 2M = 2 \left\lceil \frac{D_0(R + D_0)}{\pi} \right\rceil.$$

In [Theorem 2.1](#), we could have used one fewer term and truncated the sum to $[-M + 1, M - 1]$ instead. However, for numerical efficiency considerations, we use an even number of quadrature nodes in the Fourier spectral approximation. We have relied here on the trapezoidal rule, but the midpoint rule would also achieve spectral accuracy.

[Table 2.1](#) lists the number of terms $n_f(R)$ for various values of the precision ε and the range R . For the new version of the point FGT, we can control box dimensions so that the relevant value of R is always $2D_0$. For the continuous FGT, where an adaptive tree is provided as input, we make use of the user-provided data structure and, with dyadic refinement, can only enforce that R falls in the interval $[2D_0, 4D_0]$.

2.2. The periodic kernel. In order to impose periodic boundary conditions on a box of length 1 centered at the origin, we can replace the free-space Gaussian with an infinite set of images to obtain the periodic kernel in the form

$$(2.16) \quad G_p(x; \delta) = \sum_{m=-\infty}^{\infty} e^{-\frac{(x+m)^2}{\delta}}.$$

Note that δ can be suitably rescaled if periodic conditions are to be imposed on a box of length L . Using Fourier analysis, on the other hand, we can also write the periodic kernel as

$$(2.17) \quad G_p(x; \delta) = \sqrt{\pi\delta} \sum_{n=-\infty}^{\infty} e^{-(\pi\sqrt{\delta}n)^2} e^{i2\pi nx}.$$

Table 2.1: Number of terms needed in the Fourier spectral approximation of the Gaussian for the interval $|x| \leq R\sqrt{\delta}$ with $R = 2D_0, 3D_0$ and $4D_0$ as a function of the precision ε .

ε	D_0	$n_f(2D_0)$	$n_f(3D_0)$	$n_f(4D_0)$
10^{-2}	2.39	12	16	20
10^{-4}	3.21	20	28	34
10^{-6}	3.86	30	38	48
10^{-8}	4.42	38	50	64
10^{-10}	4.91	48	62	78
10^{-12}	5.36	56	74	92

Table 2.2: Number of terms needed in the Fourier series approximation of the periodic Gaussian on the unit interval.

$\delta \backslash \varepsilon$	10^{-2}	10^{-4}	10^{-6}	10^{-8}	10^{-10}	10^{-12}
10^{-1}	3	4	4	5	5	6
10^{-2}	7	10	12	14	16	17
10^{-3}	22	31	38	44	49	53

The equivalence of the two formulas (2.16) and (2.17) can be proven using the Poisson summation formula. It is straightforward to verify that the infinite series is well-approximated by a finite sum to precision ε ,

$$(2.18) \quad G_p(x; \delta) = \sqrt{\pi\delta} \sum_{n=-n_p}^{n_p} e^{-(\pi\sqrt{\delta}n)^2} e^{i2\pi nx} + O(\varepsilon),$$

with

$$(2.19) \quad n_p = \left\lceil \frac{\sqrt{\log(1/\varepsilon)}}{\pi\sqrt{\delta}} \right\rceil.$$

Table 2.2 lists the values of n_p for various values of ε and δ . As $\delta \rightarrow 0$, the full Fourier series for the periodic Gaussian on the unit interval requires more and more terms. However, once $\delta < 1/36$, the contribution of images beyond the first neighbors is approximately 10^{-16} , so that only a minor modification of the free-space FGT is needed for such cases (see section 5).

2.3. The non-uniform fast Fourier transform. In order to construct plane-wave representations from a collection of Gaussian sources, we will use the NUFFT in \mathbb{R}^d . For this, let n_f denote the number of desired Fourier modes in each dimension $i = 1, \dots, d$, which we have assumed to be even. Let $\mathcal{I}_{n_f} = \{-n_f/2, \dots, n_f/2 - 1\}$, then $\mathcal{I} = \mathcal{I}_{n_f} \times \dots \times \mathcal{I}_{n_f}$ contains $N = (n_f)^d$ entries. Given data points $\{\mathbf{x}_1, \dots, \mathbf{x}_M\}$, the type-1 NUFFT computes sums of the form

$$(2.20) \quad F(\mathbf{k}) = \sum_{j=1}^M f_j e^{\pm i\mathbf{k} \cdot \mathbf{x}_j},$$

where $\mathbf{k} \in \mathcal{I}$. That is, it computes the discrete Fourier transform at equispaced modes from function values at arbitrary data points. Its adjoint, also called the type-2 NUFFT evaluates sums of the form

$$(2.21) \quad f(\mathbf{x}_j) = \sum_{\mathbf{k} \in \mathcal{I}} F(\mathbf{k}) e^{\pm i \mathbf{k} \cdot \mathbf{x}_j}.$$

That is, it computes the value of a truncated Fourier series at arbitrary target points. The cost of both type-1 and type-2 NUFFTs is $O(N \log N) + O(M)$. We will make use of the FINUFFT library [1] in our implementation and refer to the paper [2] for further details and a historical review of the algorithm itself. The constant implicit in the notation $O(M)$ is roughly $(D+1)^d$ where D is the number of desired digits of accuracy and d is the dimension of the problem.

2.4. The Fourier and Gauss transforms of Legendre and Chebyshev polynomials. As we shall see below, the continuous FGT requires both the direct integration of the Gaussian kernel multiplied by a smooth function and the Fourier transform of a smooth function when using the plane wave approximation from the preceding section. In both cases, the smooth function is approximated using orthogonal polynomials on $[-1, 1]$. In particular, we will make repeated use of the integrals

$$(2.22) \quad J_\lambda[p_n](t) = \int_{-1}^1 e^{-(t-x)^2/\lambda^2} p_n(x) dx,$$

and

$$(2.23) \quad I[p_n](t) = \int_{-1}^1 e^{itx} p_n(x) dx,$$

where $p_n(x)$ is either the Legendre polynomial $P_n(x)$ or the Chebyshev polynomial $T_n(x)$ of degree n . While these could be computed numerically without a major loss of efficiency, it is convenient to do so analytically (or semi-analytically).

A five-term recurrence for $J_\lambda[p_n]$ when p_n are the Chebyshev polynomials was derived in [23]. For Legendre polynomials, the same approach leads to the following five-term recurrence,

$$(2.24) \quad \begin{aligned} \frac{n+2}{2n+3} J_\lambda[P_{n+2}](t) &= t(J_\lambda[P_{n+1}](t) - J_\lambda[P_{n-1}](t)) + \frac{(n-1)}{2n-1} J_\lambda[P_{n-2}](t) \\ &+ (2n+1) \left(\frac{\lambda^2}{2} + \frac{1}{(2n+3)(2n-1)} \right) J_\lambda[P_n](t), \quad n \geq 4. \end{aligned}$$

The first four terms in this sequence are given by

$$(2.25) \quad \begin{aligned} J_\lambda[P_0] &= \frac{\sqrt{\pi}}{2} (\operatorname{erf}(b) - \operatorname{erf}(a)), \\ J_\lambda[P_1](t) &= -\frac{d_1}{2} + t J_\lambda[P_0], \\ J_\lambda[P_2](t) &= \frac{3}{4} (-d_2 - t d_1 + (\lambda^2 - 2/3 + 2t^2) J_\lambda[P_0]), \\ J_\lambda[P_3](t) &= \frac{5}{8} (-d_1 + 2t(4J_\lambda[P_2](t) - J_\lambda[P_0])/3 - (2/5 - 4\lambda^2) J_\lambda[P_1](t)), \end{aligned}$$

where $\operatorname{erf}(x) = \frac{2}{\sqrt{\pi}} \int_0^x e^{-t^2} dt$ is the error function,

$$(2.26) \quad a = \frac{-1-t}{\lambda}, \quad b = \frac{1-t}{\lambda}, \quad d_1 = \lambda (e^{-b^2} - e^{-a^2}), \quad \text{and} \quad d_2 = \lambda (e^{-b^2} + e^{-a^2}).$$

Empirically, we observe that (2.24) appears stable for $\lambda \leq 1/8$, similar to the observation in [23] for the case of Chebyshev polynomials. For larger values of λ , the integrand is very smooth and easily computed.

As for $I[p_n]$, when p_n are Legendre polynomials, we have [14, §10.54.2]

$$(2.27) \quad I[P_n](t) = \int_{-1}^1 e^{itx} P_n(x) dx = \frac{2}{(-i)^n} j_n(t),$$

where j_n is the spherical Bessel function of order n . $I[T_n]$ can be evaluated by expanding T_n into a Legendre polynomial series and then using (2.27).

Suppose now that we are given a box B on which we have a continuous density $\sigma(\mathbf{y})$. For simplicity, we assume it is approximated by the multivariate Legendre polynomial

$$(2.28) \quad \sigma(\mathbf{y}) \approx \sum_{\|\alpha\|_\infty \leq k-1} c_\alpha P_\alpha(\mathbf{y}), \quad \mathbf{y} = (y_1, \dots, y_d) \in B.$$

Here, we are using standard multi-index notation with $\alpha = (\alpha_1, \dots, \alpha_d)$, $\|\alpha\|_\infty = \max_{i=1}^d |\alpha_i|$, $c_\alpha = c_{\alpha_1, \alpha_2, \dots, \alpha_d}$, and $c_\alpha P_\alpha(\mathbf{y}) = c_\alpha \prod_{i=1}^d P_{\alpha_i}(y_i)$, where P_n is the Legendre polynomial of degree n .

LEMMA 2.2. *The cost of computing c_α from $\sigma(\mathbf{y})$ on a tensor product grid with k^d points is $O(d k^{d+1})$.*

Proof. In one dimension, this follows from orthogonality. Using the Legendre basis (scaled to the box dimension), we have

$$(2.29) \quad c_n = \frac{2n+1}{L} \int_{-L/2}^{L/2} \sigma(y) P_n\left(\frac{2y}{L}\right) dy \approx \frac{2n+1}{2} \sum_{j=1}^k w_j \sigma(L\eta_j/2) P_n(\eta_j)$$

where L is the side length of a box, and $(\eta_j, w_j), j = 1, \dots, k$ are the nodes and weights for Gauss-Legendre quadrature on $[-1, 1]$. In higher dimensions, the result follows from the observation that one can compute this transform sequentially in each dimension, assuming σ is tabulated on a tensor product grid. \square

DEFINITION 2.3. *Let $\mathcal{T}_{val \rightarrow pol} \in \mathbb{R}^{k \times k}$ denote the one dimensional matrix from the preceding lemma which maps values of a function to its corresponding Legendre coefficients with entries*

$$\mathcal{T}_{val \rightarrow pol}(j, n) = \frac{2n+1}{2} w_n P_{j-1}(\eta_n) \quad j, n = 1, 2, \dots, k.$$

The following lemma will be used when we wish to directly compute the Gauss transform on a single box at a collection of target points.

LEMMA 2.4. *Let B be a box of side length L (assumed to be centered at the origin for simplicity of notation). Let T be a box in its neighbor list (see Definition 3.1 and Figure 4.1). Then, for a source density on B of the form (2.28), the potential at*

$\mathbf{x} = (x_1, \dots, x_d)$ is given by

$$\begin{aligned}
 u(\mathbf{x}) &= \int_B e^{\|\mathbf{x}-\mathbf{y}\|^2/\delta} \sigma(\mathbf{y}) d\mathbf{y} \\
 &= \sum_{\|\alpha\|_\infty \leq k-1} c_\alpha \int_B e^{\|\mathbf{x}-\mathbf{y}\|^2/\delta} P_\alpha(\mathbf{y}) d\mathbf{y} \\
 (2.30) \quad &= \left(\frac{L}{2}\right)^d \sum_{\|\alpha\|_\infty \leq k-1} c_\alpha J_\lambda[P_{\alpha_1}](2x_1/L) \cdots J_\lambda[P_{\alpha_d}](2x_d/L)
 \end{aligned}$$

where $\lambda = 2\delta/L$ and $J_\lambda[P_n](x)$ is given by (2.22).

Proof. The formula follows immediately from (2.22), (2.28), and the change of variables $y_i \rightarrow 2y_i/L$ to rescale the box B to one of dimension $[-1, 1]^d$. \square

REMARK 2.5. Assuming the output points $\{\mathbf{x}_i, i = 1, \dots, k^d\}$ lie on a tensor-product grid in d dimensions, separation of variables can be used to accelerate the evaluation of (2.30) at all targets. It is easy to check that the cost of evaluation is $O(dk^{d+1})$ floating point operations.

It is also straightforward to expand the Gauss transform over a box with a polynomial density in the plane wave basis (assuming that the interaction is within the cutoff range so that the plane wave approximation is accurate).

LEMMA 2.6. Let B be a box of side length L centered at the origin and let T be a target box where the potential induced by the source density σ is to be evaluated. Then

$$\begin{aligned}
 u(\mathbf{x}) &= \int_B e^{\|\mathbf{x}-\mathbf{y}\|^2/\delta} \sigma(\mathbf{y}) d\mathbf{y} \\
 &= \sum_{\|\alpha\|_\infty \leq k-1} c_\alpha \int_B e^{\|\mathbf{x}-\mathbf{y}\|^2/\delta} P_\alpha(\mathbf{y}) d\mathbf{y} \\
 &= \sum_{m_1=-n_f/2}^{n_f/2-1} \cdots \sum_{m_d=-n_f/2}^{n_f/2-1} e^{-i\mathbf{h}\mathbf{m}\cdot\mathbf{x}/\sqrt{\delta}} v(\mathbf{m})
 \end{aligned}$$

where $\mathbf{m} = (m_1, \dots, m_d)$ and

$$v(\mathbf{m}) = \left(\frac{L}{2}\right)^d e^{-\|\mathbf{m}\|^2 h^2/4} \sum_{\|\alpha\|_\infty \leq k-1} c_\alpha I[P_{\alpha_1}]\left(\frac{Lm_1 h}{2\sqrt{\delta}}\right) \cdots I[P_{\alpha_d}]\left(\frac{Lm_d h}{2\sqrt{\delta}}\right)$$

where $I[P_n](x)$ is given by (2.23) and h is given in (2.4).

Proof. The formula follows from (2.28), (2.23), Theorem 2.1, and a change of variables mapping B to the box $[-1, 1]^d$. \square

REMARK 2.7. Lemma 2.6 will be used to accelerate the calculation of Gaussian interactions at fine levels in the FGT hierarchy. It is easy to verify that, using separation of variables, the cost is $O(n_f k)$ in one dimension, $O(n_f k^2 + n_f^2 k)$ in two dimensions, and $O(n_f k^3 + n_f^2 k^2 + n_f^3 k)$ in three dimensions. For the values of n_f and k that are of practical interest, this is more efficient than using the NUFFT.

Having formed a plane wave expansion, it can be evaluated efficiently on a tensor product grid (within the relevant range).

LEMMA 2.8. *Let B be a box of side length L centered at the origin. Then*

$$u(\mathbf{x}) = \sum_{m_1=-n_f/2}^{n_f/2-1} \cdots \sum_{m_d=-n_f/2}^{n_f/2-1} e^{-i\mathbf{h}\mathbf{m}\cdot\mathbf{x}/\sqrt{\delta}} v(\mathbf{m})$$

can be evaluated on a tensor product grid using $O(n_f k)$ operations in one dimension, $O(n_f k^2 + n_f^2 k)$ operations in two dimensions, and $O(n_f k^3 + n_f^2 k^2 + n_f^3 k)$ operations in three dimensions.

3. The new discrete FGT. We turn now to the fast Gauss transform for point sources $\{\mathbf{y}_j, j = 1, \dots, N\}$ and targets $\{\mathbf{x}_i, i = 1, \dots, M\}$ in free space. For a prescribed precision ε , we first determine the “cutoff” length $D_0\sqrt{\delta}$ via (2.2). We then construct an adaptive level-restricted tree so that $D_0\sqrt{\delta}$ is the exact dimension of a leaf node at some level of refinement. For this, we first determine the median of the point distribution $\mathbf{x}_0 = (x_{0,1}, \dots, x_{0,d}) \in \mathbb{R}^d$, with

$$(3.1) \quad x_{0,k} = X_k^{max} - X_k^{min}$$

where

$$X_k^{max} = \max_{k=1}^d (\max_{i=1}^M x_{i,k}, \max_{j=1}^N y_{j,k}),$$

$$X_k^{min} = \min_{k=1}^d (\min_{i=1}^M x_{i,k}, \min_{j=1}^N y_{j,k}).$$

We set \mathbf{x}_0 to be the center of the “root” node B_0 . The side length L_0 of the (square) root node is defined to be the smallest value

$$(3.2) \quad L_0 = 2^{l_c} D_0 \sqrt{\delta}$$

which contains all the sources and targets, where $l_c \in \mathbb{Z}^+$. We will refer to l_c as the “cutoff” level. We then build a *level-restricted* adaptive tree that sorts the sources and targets and refines boxes until each leaf node either has fewer than n_s sources and targets or the tree has reached the cutoff level. Here n_s is a user-supplied constant. We use the standard language of tree data structures, with level 0 defined to be the root node itself, and level $l+1$ obtained recursively by subdividing each box at level l into 2^d equal parts. If B is a box at level l , the 2^d boxes at level $l+1$ obtained by its subdivision are referred to as its children.

DEFINITION 3.1. *A tree is called level-restricted or balanced if two leaf nodes that share a boundary point are at most one level apart in the hierarchy (Figure 3.1). In a level restricted tree, for any leaf node B at level l , the leaf nodes sharing a boundary point at the same level are called colleagues (including B itself). The leaf nodes at level $l+1$ sharing a boundary point with B are called fine neighbors and the leaf nodes at level $l-1$ sharing a boundary point with B are called coarse neighbors. The union of these three sets of boxes is called the neighbor list.*

The tree construction is carried out by the following method, where by *points*, we mean the union of sources and targets.

DEFINITION 3.2. *The P-list of a box B , denoted by $L_P(B)$, consists of all colleagues containing more than n_s points. Note that the P-list is non-empty for boxes B at the cut-off level only. The D-List of a leaf node B at any level, denoted by $L_D(B)$, consists of all members of the neighbor list that are not in $L_P(B)$.*

Algorithm 3.1 Construction of level-restricted adaptive tree

On input, we are given a collection of N sources \mathbf{y}_j , $j = 1, 2, \dots, N$, a collection of M targets \mathbf{x}_i , $i = 1, 2, \dots, M$, and n_s the maximum number of points in a box. The output is a level-restricted adaptive tree which has sorted the sources and targets.

► Determine the center \mathbf{x}_0 of the root node B_0 , the box size L_0 and the cutoff length $D_0\sqrt{\delta}$, as above.

For $l = 0, 1, \dots, l_c - 1$

For each nonempty box B_i at level l

If Number of sources or targets in $B_i > n_s$ then

► Subdivide B_i into 2^d child boxes at level $l + 1$

► Assign each point in B_i to the child box in which is contained

End

End

End

► If the resulting adaptive tree is not level-restricted, add additional refinement to enforce the condition using standard algorithms (see, for example, [19]). For the discrete FGT, also ensure that a leaf node at the cutoff level containing more than n_s points has no coarse neighbors.

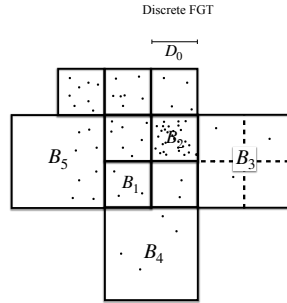


Fig. 3.1: An adaptive tree for the discrete FGT. The tree is used to resolve the point distribution down to the cutoff level, where the box dimension is $D_0\sqrt{\delta}$. In this illustration, B_2 , a box at the cutoff level contains more than n_s points with a coarse neighbor B_3 . This forces refinement, even though B_3 had fewer than n_s sources, in order to satisfy the criterion that the densely populated leaf node B_2 has no coarse neighbors. Note that boxes B_4, B_5 do not require refinement. This will permit us to compute all non-trivial interactions for the points in B_2 using plane wave representations.

In the new FGT, all processing is carried out at the cutoff level (or above). For a target point \mathbf{x} in a box B , the corresponding potential $u(\mathbf{x})$ can be approximated by the sources in $L_D(B)$ and $L_P(B)$ with an error of $O(\varepsilon)$, because of the exponential decay of the Gaussian, i.e.,

$$(3.3) \quad u(\mathbf{x}) \approx u_D + u_P = \sum_{\mathbf{y}_j \in L_D(B)} G(\mathbf{x} - \mathbf{y}_j; \delta) q_j + \sum_{\mathbf{y}_j \in L_P(B)} G(\mathbf{x} - \mathbf{y}_j; \delta) q_j,$$

For sources in $L_D(B)$, we compute the sum directly. It is straightforward to verify that, in a level-restricted tree, there are at most $C_d = 4^d - 2^d$ neighbors for any box (the maximum corresponding to a box at level l surrounded by fine neighbors at level

$l + 1$). Since each box in $L_D(B)$ contains at most n_s sources, the cost of evaluating the first sum in (3.3) is bounded by a constant of the order $O(C_d n_s)$.

For the second term u_P in (3.3), we will approximate the Gaussian field using a plane-wave approximation, following Theorem 2.1. In d dimensions, we use the tensor product version of the formula, given by

$$(3.4) \quad G(\mathbf{x} - \mathbf{y}; \delta) \approx \sum_{l=1}^{N_F} w_l e^{i\mathbf{k}_l \cdot (\mathbf{x} - \mathbf{y})}.$$

Here, $N_F = n_f(2D_0)^d$ with $n_f(2D_0)$ given in the third column of Table 2.1 and $\mathbf{k}_l, l = 1, \dots, N_F$ are the uniformly spaced points on a tensor product grid in Fourier space. Recall, from the discussion in subsection 2.1, that the formula (3.4) is accurate so long as $|x_i - y_i| \leq 2D_0\sqrt{\delta}$ for $i = 1, \dots, d$. Letting \mathbf{c}_T be the center of box T containing target \mathbf{x} , and \mathbf{c}_S the center of box S in $L_P(B)$, we define the *outgoing* expansions $\phi_l(S), l = 1, \dots, N_F$ and the *incoming* expansions $\psi_l(B), l = 1, \dots, N_F$ by

$$(3.5) \quad \phi_l(S) = \sum_{\mathbf{y}_j \in S} e^{-i\mathbf{k}_l \cdot (\mathbf{y}_j - \mathbf{c}_S)} w_l q_j, \quad l = 1, \dots, N_F,$$

and

$$(3.6) \quad \psi_l(T) = \sum_{S \in L_P(T)} e^{i\mathbf{k}_l \cdot (\mathbf{c}_T - \mathbf{c}_S)} \phi_l(S). \quad l = 1, \dots, N_F,$$

respectively. It is straightforward to see that the contribution to u_P at the target point $\mathbf{x} \in T$ is

$$(3.7) \quad u_P(\mathbf{x}) = \sum_{l=1}^{N_F} e^{i\mathbf{k}_l \cdot (\mathbf{x} - \mathbf{c}_T)} \psi_l(T).$$

Thus, the NUFFT-based discrete FGT is described by the following five steps.

Let N_{box} denote the number of boxes B_i which have greater than n_s sources. The cost of forming outgoing expansions is $O(N_{box} N_F \log(N_F) + \log^d(1/\varepsilon)N)$, the cost of gathering expansions is $O(3^d N_{box} N_F)$, and the cost of evaluating expansions is $O(N_{box} N_F \log(N_F) + \log^d(1/\varepsilon)M)$. Finally, the cost of the direct interactions is bounded by $O((4^d - 2^d)n_s M)$. Since N_F is $O(\log^d(1/\varepsilon))$ by Theorem 2.1, the total cost of the point FGT is

$$(3.8) \quad O\left(\log^d(1/\varepsilon)(M + N)\right).$$

For readers familiar with previous planewave-based FGT algorithms, it is worth noting that the expansion length N_F is the same. Moreover, the total number of translations per box is not much greater than in the sweeping method of [11, 16, 17], but permits a simple implementation on an adaptive tree.

REMARK 3.3. *It is also worth considering two extremes. When $\delta \rightarrow 0$, the range of influence of a Gaussian is vanishingly small. In that case, virtually no expansion-related work is carried out, and the FGT basically serves as an adaptive algorithm that assists in the determination of near neighbors for direct calculation. When $\delta \rightarrow \infty$, on the other hand, the Gaussian becomes smoother and smoother and the algorithm becomes trivial. The tree construction terminates at the level of the root node, and the FGT carries out one type-1 NUFFT and one type-2 NUFFT.*

Algorithm 3.2 NUFFT-based point FGT

On input, the set of N sources and M targets are assumed to be sorted on a level restricted adaptive tree, as described in [Algorithm 3.1](#), for refinement parameter n_s . The output is the potential evaluated at all target locations.

```

For each box  $B_i$  at level  $l_c$                                      (Form outgoing expansion)
  If Number of sources in  $B_i > n_s$  then
    ▶ Form the outgoing expansion  $\phi_\ell(B_i)$  from sources in  $B_i$  according to (3.5)
      using the type-1 NUFFT.
  End
  ▶ Initialize the incoming expansion  $\psi_l(B_i)$  to zero.
End
For each nonempty box  $B_i$  at level  $l_c$                          (Gather expansions)
  ▶ Translate outgoing expansion for each box  $S \in L_P(B_i)$  to the center of  $B_i$  and
  add to the incoming expansion  $\psi_l(B_i)$  according to (3.6). (Each such translation
  is in diagonal form requiring only  $N_F$  complex multiplications.)
End
For each nonempty leaf box  $B_i$  at level  $l_c$                    (Evaluate incoming expansions)
  ▶ Evaluate  $\psi_l(B_i)$  at all targets in  $B_i$  according to (3.7), using the type-2
  NUFFT.
End
For  $l = 0, \dots, l_c$                                          (Direct interaction)
  For each leaf box  $B_i$  at level  $l$ 
    ▶ Compute the direct influence of the sources in  $B_i$  at all targets in every
    box  $B_j$  in  $L_D(B_i)$ .
  End
End

```

REMARK 3.4. For step 5 of the FGT (direct evaluation), a simple optimization is to consider only the sources that lie in a ball of radius $D_0\sqrt{\delta}$ centered at each target point rather than all sources lying in the near neighbors. In three dimensions, this reduces the cost by a factor of two or so.

4. The box FGT. We now consider the evaluation of the continuous or box Gauss transform (1.2), where the density $\sigma(\mathbf{x})$ is assumed to be smooth and resolved on a level-restricted tree. We briefly describe how to construct such a tree given a user-provided function that can evaluate σ at any arbitrary point. For this, let k denote the desired polynomial order of approximation in each dimension and let ε be the desired precision. Let L_0 denote the side length of the root box B_0 which we assume is centered at the origin. Given an adaptive tree superimposed on B_0 , we approximate the density $\sigma(\mathbf{x})$ on any box B in this hierarchical data structure as discussed in (2.28), i.e.,

$$\sigma(\mathbf{x}) \approx \sum_{\|\alpha\|_\infty \leq k-1} c_\alpha p_\alpha(\mathbf{x}), \quad \mathbf{x} = (x_1, \dots, x_d) \in B.$$

It is well-known that the approximation error in (2.28) can be estimated from the tails of the coefficients c_α outside the l_2 ball as

$$(4.1) \quad e = \sqrt{\frac{1}{N_{k,2}} \sum_{\|\alpha\|_2 \geq k} |c_\alpha|^2},$$

where $N_{k,2}$ is the number of terms in the summation. (See, for example, [21, 22].) Using this error monitor, it is straightforward to recursively build an adaptive tree that resolves the density σ .

Algorithm 4.1 Resolving a continuous density on a level-restricted adaptive tree

Input is a tolerance ε , and the density function σ which can be evaluated at an arbitrary point. We assume that a Legendre basis is used to represent the density on each box. The output is a level-restricted adaptive tree which resolves σ to precision ε .

For level $l = 0, 1, \dots$

For each box B_i at level l

- ▶ Compute the density at the tensor product Legendre nodes in B_i .
- ▶ Calculate the expansion coefficient vector c_α using (2.29), Lemma 2.2.
- ▶ Estimate the approximation error $e(B_i)$ via (4.1).

If $e(B_i) > \varepsilon \|\sigma\|_2$ then

- ▶ Subdivide B_i into 2^d child boxes at level $l + 1$

End

End

End

- ▶ If the resulting adaptive tree is not level-restricted, add additional refinement to enforce the condition using standard algorithms (see, for example, [19]). The density on the refined boxes can be obtained either by interpolation or by calling the user-provided function. If we let N_{leaf} denote the number of leaf nodes, then there are $N = N_{\text{leaf}} \cdot k^d$ total points in the discretization. It is easy to check that the cost of building the tree is approximately $O(dkN)$.
-

There are several important distinctions to highlight between the continuous and discrete FGTs:

1. Unlike the discrete FGT, the tree construction does not terminate at the cutoff level l_c . Deeper levels of refinement may be needed to resolve the source density.
2. There are no empty boxes in the data structure. In regions of space where the density is smooth, refinement will terminate at a coarse level, but every leaf node is assumed to have a non-trivial density $\sigma(\mathbf{x})$ tabulated on a tensor product grid with k^d points.
3. Most importantly, we can make very effective use of separation of variables at every step of the algorithm, using the tools developed in subsection 2.4 and illustrated in Figure 4.1, as we shall now see.

4.1. Precomputation. Before turning to the algorithm itself, we define several matrices that will be used throughout the box FGT and need to be computed once per level. It is straightforward to see that, in a level-restricted tree, the tensor product grids on neighbors can only have a few possible locations with respect to a source leaf box B . As illustrated in Figure 4.1, assuming B is of side length L , the offset of the center of any fine neighbor in the x_1 direction has only four possible values: $\{-3L/4, -L/4, L/4, 3L/4\}$, which we denote by s_1, s_2, s_3, s_4 , respectively.

DEFINITION 4.1. Letting $\xi_1^{s_l}, \dots, \xi_k^{s_l}$ be the k Legendre nodes scaled to the fine neighbor length $L/2$, and offset by the relevant value $s_l, l = 1 \dots, 4$, we define by $\mathcal{T}_{\text{pol} \rightarrow \text{pot}}^{s_l} \in \mathbb{R}^{k \times k}$ the one dimensional matrix $\mathcal{T}_{\text{pol} \rightarrow \text{pot}}^{s_l} \in \mathbb{R}^{k \times k}$ with entries

$$\mathcal{T}_{\text{pol} \rightarrow \text{pot}}^{s_l}(i, j) = J_\lambda[P_{j-1}](2\xi_i^{s_l}/L),$$

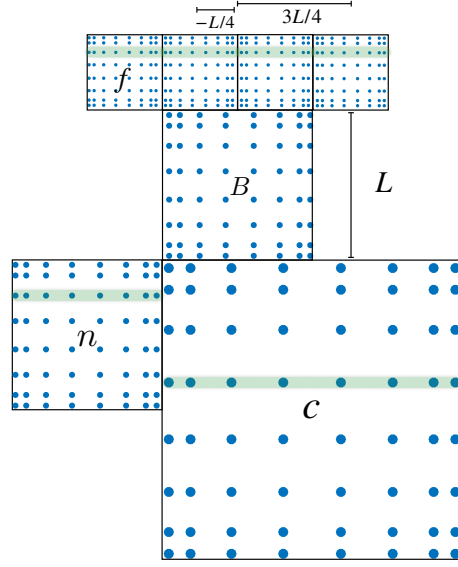


Fig. 4.1: For a leaf node B at a coarse level, its interactions with neighbors are computed directly. There are only a finite number of possible locations for colleagues (n), fine neighbors (f) and coarse neighbors (c). More precisely, it is straightforward to see that in d dimensions, there are at most 3^d colleagues, $(2^d - 1) \cdot 2^d$ fine neighbors and $(2^d - 1) \cdot 2^d$ coarse neighbors. Because of the separability of the Gaussian and the fact that the target grids are defined as tensor products, the cost of direct calculation is $O(dk^{d+1})$ rather than $O(k^{2d})$, where k^d is the number of grid points in a box. Note also that, in a level-restricted tree, the tensor product grids on neighbors can only have a few possible locations with respect to a leaf box B . Assuming B is of side length L , the offset of the center of any fine neighbor in the x_1 -direction has only four possible values: $\{-3L/4, -L/4, L/4, 3L/4\}$.

where $\lambda = 2\delta/L$ for $i, j = 1, \dots, k$.

Likewise, the center of a coarse neighbor also has only four possible values: $\{-3L/2, -L/2, L/2, 3L/2\}$, which we denote by s_5, s_6, s_7, s_8 , respectively.

DEFINITION 4.2. $\mathcal{T}_{pol \rightarrow pot}^{s_l}$ for $l = 5, \dots, 8$ is defined as for fine neighbors but with $\{\xi_i\}$ located at scaled Legendre grid points on a coarse neighbor with offset s_l .

The center of a colleague has only three possible values: $\{-L, 0, L\}$, which we denote by s_9, s_{10}, s_{11} , respectively.

DEFINITION 4.3. $\mathcal{T}_{pol \rightarrow pot}^{s_s}$ for $s = 9, 10, 11$ is defined as for other neighbors but with $\{\xi_i^{s_i}\}$ located at a scaled Legendre grid on a colleague with offset s_l .

The total cost at each level is negligible — just $11k^2$ evaluations of the function $J_\lambda[P_{j-1}]$.

We will also make repeated use of the one-dimensional transformation matrices $\mathcal{T}_{pol \rightarrow pw}$ which map polynomial basis functions to their plane-wave expansion coefficients via (2.23).

DEFINITION 4.4. We define $\mathcal{T}_{pol \rightarrow pw} \in \mathbb{C}^{n_f \times k}$ as the matrix with entries

$$\mathcal{T}_{pol \rightarrow pw}(i, j) = I[P_{j-1}](Lih/(2\sqrt{\delta})),$$

where h is given in (2.4).

Once the plane wave expansions are available for a box B , we will make use of the precomputable matrices $T_{pw \rightarrow pot}$ for evaluation.

DEFINITION 4.5. We define $\mathcal{T}_{pw \rightarrow pot} \in \mathbb{C}^{k \times n_f}$ as the matrix with entries

$$\mathcal{T}_{pw \rightarrow pot}(n, m) = e^{-ihm\xi_n/\sqrt{\delta}},$$

where h is given in (2.4) and the $\{\xi_i\}$ are the Legendre nodes scaled to the box's side length L , according to (2.8).

Given a plane wave expansion for a box B of the form

$$u(\mathbf{x}) = \sum_{\mathbf{m}} e^{-ih\mathbf{m} \cdot \mathbf{x}/\sqrt{\delta}} v(\mathbf{m})$$

we will also need to shift the expansion center to either a parent, child or colleague. We have already encountered the ‘‘outgoing to incoming’’ shift in (3.6). We define the corresponding map as the diagonal matrix $\mathcal{T}_{out \rightarrow in} \in \mathbb{C}^{N_F \times N_F}$ with non-zero entries $\mathcal{T}_{out \rightarrow in}(l, l) = e^{i\mathbf{k}_l \cdot (\mathbf{c}_B - \mathbf{c}_S)}$, where \mathbf{c}_B is the center of B and \mathbf{c}_S is the center of its colleague. When shifting an outgoing expansion from child to parent, we will use the diagonal matrix $\mathcal{T}_{c \rightarrow p} \in \mathbb{C}^{N_F \times N_F}$ with non-zero entries $\mathcal{T}_{c \rightarrow p}(l, l) = e^{-i\mathbf{k}_l \cdot (\mathbf{c}_S - \mathbf{c}_B)}$, where \mathbf{c}_S is the center of one of B 's children. For the reverse, shifting an incoming expansion from parent to child, we will use the diagonal matrix $\mathcal{T}_{p \rightarrow c} \in \mathbb{C}^{N_F \times N_F}$ with non-zero entries $\mathcal{T}_{p \rightarrow c}(l, l) = e^{i\mathbf{k}_l \cdot (\mathbf{c}_B - \mathbf{c}_S)}$, where \mathbf{c}_S is the center of B 's child. Aspects of the box FGT are shown in Figure 4.2.

4.2. The full algorithm. As noted above, the box FGT is a little more involved than the discrete FGT, since the tree construction does not terminate at the cutoff level l_c . Because of the separability of all steps in the algorithm, however, the performance in terms of work per grid point is significantly better. The algorithm combines hierarchical aspects of the FMM with the plane wave approach of [11, 17].

DEFINITION 4.6. The *P-List*, $L_P(B)$, of a non-leaf box at level l_c consists of all of its non-leaf neighbors at level l_c . The *D-List*, $L_D(B)$, of a leaf box at level $l \leq l_c$ consists of all of its leaf neighbors at level $l \leq l_c$.

DEFINITION 4.7. For each box B , we also assign a flag $f(B)$ that indicates whether it requires storage for a plane-wave expansion. We set $f(B) = 1$ if it does: either because it is at a level $l > l_c$ or because it is at level l_c and one of its colleagues is further subdivided.

A somewhat tedious calculation shows that the total computational cost is bounded by

$$(4.2) \quad C \leq c_1 N_{\text{leaf}} n_f^d k + c_2 N_b n_f^d + c_3 3^d N_b n_f^d + c_4 3^d d k^{d+1} N_{\text{leaf}},$$

where N_{leaf} is the number of leaf nodes, n_f is the number of plane wave modes in one dimension, and N_b is the total number of boxes in the adaptive tree.

Using the fact that $N_b \leq \frac{1}{1-2^{-d}} N_{\text{leaf}}$, and that the total number of tensor product grid points is $N = N_{\text{leaf}} k^d$, we have

$$(4.3) \quad C = O\left([k(n_f/k)^d + 3^d(n_f/k)^d + 3^d k] N\right).$$

Algorithm 4.2 The box FGT

On input, the source density is assumed to be provided on a level-restricted adaptive tree with k th order tensor product data on leaf nodes, as constructed in [Algorithm 4.1](#), with cutoff level l_c and maximum refinement level l_{\max} . The output is the potentials evaluated at all tensor product grid points on all leaf boxes.

```

For level  $l = l_{\max}, l_c, -1$  (Form outgoing expansions)
  ▶ Compute the operators  $\mathcal{T}_{pol \rightarrow pw}$  and  $\mathcal{T}_{val \rightarrow pw} = \mathcal{T}_{val \rightarrow pol} \mathcal{T}_{pol \rightarrow pw}$  for level  $l$ 
  (Definitions 2.3 and 4.4).
  For each leaf box  $B_i$  with  $f(B_i) = 1$  at level  $l$ 
    ▶ Transform function values in  $B_i$  to the plane-wave expansion using
       $\mathcal{T}_{val \rightarrow pw}$ .
  End
End
For level  $l = l_{\max} - 1, l_c, -1$  (Merge outgoing expansions)
  ▶ Compute the operators  $\mathcal{T}_{c \rightarrow p}$  for level  $l + 1$ .
  For each non-leaf box  $B_i$  at level  $l$ 
    ▶ Translate and merge the plane-wave expansions of its children using  $\mathcal{T}_{c \rightarrow p}$ .
  End
End
▶ Compute the operators  $\mathcal{T}_{out \rightarrow in}$  for level  $l_c$ .
For each box  $B_i$  at level  $l_c$  (Gather expansions)
  For each box  $S$  in  $L_P(B_i)$ 
    ▶ Merge the outgoing expansion  $\phi(S)$  into the incoming expansion  $\psi(B_i)$ 
    using  $\mathcal{T}_{out \rightarrow in}$ .
  End
End
For level  $l = l_c, \dots, l_{\max} - 1$  (Push to children)
  ▶ Compute the operators  $\mathcal{T}_{p \rightarrow c}$  for level  $l$ .
  For each non-leaf box  $B_i$  with  $f(B_i) = 1$  at level  $l$ 
    ▶ Translate the incoming expansion  $\psi(B_i)$  to its children using  $\mathcal{T}_{p \rightarrow c}$ .
  End
End
For level  $l = l_c, \dots, l_{\max}$  (Evaluate expansion)
  ▶ Compute the operator  $\mathcal{T}_{pw \rightarrow pot}$  for level  $l$ .
  For each leaf box  $B_i$  at level  $l$ 
    ▶ Evaluate the expansion  $\psi(B_i)$  at the tensor product grid using  $\mathcal{T}_{pw \rightarrow pot}$ .
  End
End
For  $l = 0, \dots, l_c$  (Direct interaction)
  For each source box  $S$  at level  $l$ 
    ▶ Compute the operators  $\mathcal{T}_{pol \rightarrow pot}^{s_j}$ ,  $j = 1, 2, \dots, 11$ , and  $\mathcal{T}_{val \rightarrow pot} =$ 
 $\mathcal{T}_{val \rightarrow pol} \mathcal{T}_{pol \rightarrow pot}$  for level  $l$ .
    For each target box  $T$  in  $L_D(S)$ 
      ▶ Compute the influence of  $S$  at targets in  $T$  using  $\mathcal{T}_{val \rightarrow pot}$  and add to
      the contribution from the evaluation of local expansions.
    End
  End
End
End

```

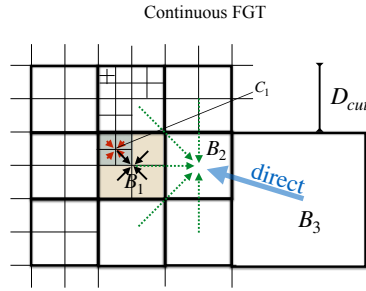


Fig. 4.2: In the box FGT, outgoing plane wave expansions are recursively merged from fine levels up to the cutoff level (where boxes are of side length D_{cut}), illustrated for box B_1 and its refined child C_1 . Outgoing expansions are first translated along the red arrows to the center of C_1 from its children. The black arrows indicate merger at the next level, resulting in the outgoing expansion for B_1 . Once all outgoing expansions are available at the cutoff level, they are translated to incoming expansions. This is illustrated for box B_2 . It acquires incoming expansions from its *colleagues* (green dashed arrows) but the contribution from the source density in the coarse neighbor B_3 is obtained directly, using precomputed tables and separation of variables (thick blue arrow). Returning to a consideration of box B_1 , once it has acquired all relevant data as an incoming expansion, that expansion is pushed recursively to its children until leaf nodes are reached, at which point the plane wave expansion is evaluated on the tensor product grid.

4.3. Resolving the output potential. After completing the box FGT, we have accurately computed the potential at the given tensor product grid to the requested precision. In many applications, however, one needs to evaluate the potential at auxiliary target points. If the adaptive tree that resolves the input source density were sufficient to resolve the output potential as well, then one could simply use polynomial interpolation for these points. It is perhaps surprising that, *in an adaptive environment*, this is not always the case, despite the fact that convolving with a Gaussian is a smoothing operator. This phenomenon is best illustrated with a two-dimensional example. In Figure 4.3, we show an adaptive tree resolving a source distribution (top left) and the adaptive tree needed to resolve the convolution of that distribution with a Gaussian. The difficulty here is that a sharp feature can be diffused a short distance while remaining too sharp to be well resolved by the original adaptive grid. In this example, the input data consists of two sharply peaked Gaussians

$$\sigma_f(\mathbf{x}) = \sum_{i=1}^2 e^{-\|\mathbf{x}-\mathbf{x}_i\|^2/\alpha_i}$$

with $\alpha_1 = \alpha_2 = 10^{-4}$. We let $\delta = 4 \times 10^{-3}$, and set the polynomial approximation order to $k = 8$ and the requested precision to $\varepsilon = 10^{-12}$. We then evaluate the potential at four million equispaced tensor product points on the unit box. A level-restricted adaptive tree is constructed resolve the input data to the requested precision. The total number of boxes is 5,709 and among them 4,282 are leaf boxes. If we use the potential values at the tensor grid of the input tree to calculate the potentials at four million equispaced points by interpolation. The relative l_2 error is about 10^{-7} . To remedy this loss of precision, we introduce refinement (and coarsening) capabilities

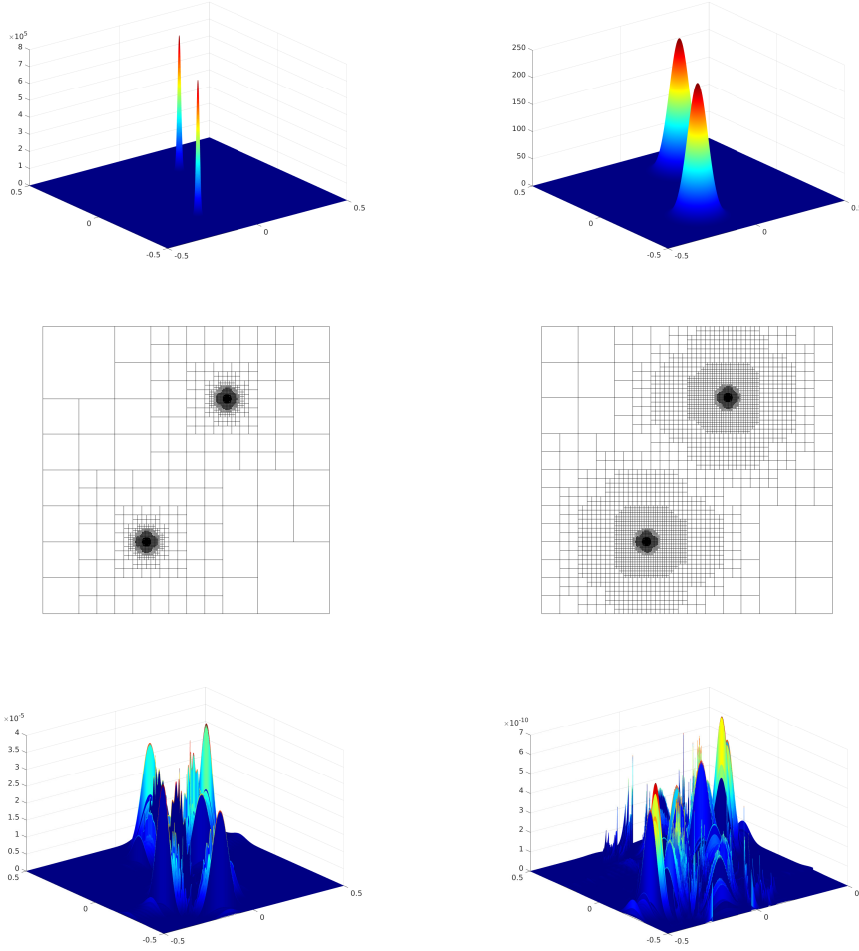


Fig. 4.3: Illustration of the necessity of a new output tree for potential evaluation at arbitrary targets by local polynomial interpolation. Top left: the input data. Top right: the output potential (i.e., the Gauss transform of the input data). Middle left: the quadtree that resolves the input data to 12 digits of accuracy. Middle right: the quadtree that resolves the output potential to 12 digits of accuracy. Bottom left: the absolute errors of the potentials at four million equispaced target points using the input quadtree (y -axis in 10^{-5} scale); Bottom right: the absolute errors of the potentials at four million equispaced target points using the correct output quadtree (y -axis in 10^{-10} scale).

below. After refinement, the relative l_2 error is about 1.3×10^{-12} . During the refinement stage, 3,400 boxes are added. During the coarsening stage, 3,824 boxes are deleted. Enforcing the level-restriction added only 16 boxes and the total number of boxes in the new tree is 5,301.

The refinement algorithm, guaranteeing that the output is resolved to any requested precision, is straightforward (Algorithm 4.3).

REMARK 4.8. *Algorithm 4.3* may require operators such as $T_{pol \rightarrow pot}$ for boxes

Algorithm 4.3 Tree refinement

On input, we have an adaptive, level-restricted tree T_0 with N_0 boxes, that resolves the density σ and for which we have computed the potential u on a tensor product grid of order k for each leaf node, using [Algorithm 4.2](#). On output, we obtain a new adaptive tree T_1 obtained by recursive subdivision ensuring that the potentials on each leaf node are well approximated by tensor product polynomial approximation to the prescribed precision ε .

- ▶ Create an integer array `ifrefine` of sufficient length $N_{\max} \gg N_0$ and initialize it to zero.
 - For box $i = 1, \dots, N_0$
 - If B_i is a leaf box then
 - ▶ Convert function values at the tensor product grid to the corresponding polynomial expansion using [Lemma 2.2](#).
 - ▶ Calculate the estimated approximation error $e(B_i)$ via [\(4.1\)](#).
 - If $e(B_i) > \varepsilon$ then
 - ▶ `ifrefine`(B_i) = 1.
 - End
 - End
 - For box $i = 1, 2, \dots$
 - If (`ifrefine`(B_i) = 1) then
 - ▶ Divide B_i into 2^d child boxes and append them to the tail of the box list.
 - If ($f(B_i) = 1$) from [Definition 4.7](#) then,
 - ▶ Translate the plane-wave expansion $\psi(B_i)$ to its children.
 - End
 - ▶ Evaluate the translated expansion at the tensor product grid on each child using $T_{\text{pw} \rightarrow \text{pot}}$ and add direct contributions using $T_{\text{pol} \rightarrow \text{pot}}$ if present.
 - End
 - End
 - ▶ If desired, rebalance the tree so that it is level-restricted.
-

which do not satisfy the level-restricted property. Since the tables are of dimension $k \times k$, the additional cost is negligible. Note that the maximum number of refinements for a leaf box at level l is $l_{\max} - l$. That is, maximum tree refinement can never be deeper than the tree resolving the source data.

REMARK 4.9. *The refinement algorithm requires precomputation of more local tables than those in [Definitions 4.1–4.3](#). Let N_{refine} denote the maximum number of refinements. A careful calculation shows that the total number of local tables needed is bounded by $2^{N_{\text{refine}}+2} \cdot (N_{\text{refine}} + 3) + 1$. Furthermore, instead of splitting the local tables into three categories as in [Definitions 4.1–4.3](#), one may place all local tables into one big array and retrieve the correct index of the table for a given pair of source and target boxes by calculating the ratio of the distance between their centers to $\tilde{L} = L/2^{N_{\text{refine}}+2}$, with L the side length of the source box.*

While [Figure 4.3](#) suggests that refinement can create a large number of new boxes, the mollifying behavior of the Gaussian also permits tree *coarsening* if the function is deemed to be over-resolved. The algorithm for tree coarsening is also simple and presented in [Algorithm 4.4](#).

Algorithm 4.4 Tree coarsening

On input, we are given an adaptive tree T_0 on which the potential is resolved to the prescribed precision, but may be over-resolved. On output, we have a coarsened tree T_1 that has fewer boxes but still resolves the input function.

For level $l = l_{\max} - 1, 0, -1$

For each non-leaf box B_i at level l

If all child boxes of B_i are leaf boxes then

- ▶ Convert function values at the tensor product grid to the corresponding polynomial expansion using [Lemma 2.2](#).
- ▶ Evaluate the potential at the k^d tensor product grid points on B_i based on which child the grid point is in.
- ▶ Convert function values at the grid points on B_i to the corresponding polynomial expansion using [Lemma 2.2](#).
- ▶ Compute the error estimate $e(B_i)$ using [\(4.1\)](#).
- ▶ If $e(B_i) \leq \varepsilon$, delete the children of B_i from the tree and set B_i to be a leaf node.

End

End

End

- ▶ If desired, rebalance the tree so that it is level-restricted.
-

5. Periodic boundary conditions. Periodic boundary conditions are easily implemented as follows. When $l_c \leq 1$, i.e., when δ is sufficiently large, the plane-wave expansion of the periodic Gaussian G_p on the entire box B (the root node) requires a modest number of terms and can be used directly. When $l_c \geq 2$, the influence of distant image boxes at the relevant scale is exponentially small and one can simply modify the definition of the *colleague* list by include one layer of image boxes around B at the cutoff level. Lists L_D and L_P also require slight modification to take the additional neighbors into account.

6. Numerical results. In this section, we illustrate the performance of the new FGTs for discrete and continuous sources. The code is written in Fortran and compiled using gfortran 9.4.0 with optimization flag -O3. All experiments were run in single-threaded mode on a 2.40GHz Intel(R) i9-10885H CPU. We will present numerical results in two and three dimensions, because the one-dimensional results don't reveal any additional interesting features.

6.1. Point FGT experiments. From the cost breakdown discussed just before the estimate [\(3.8\)](#), it is easy to see that the performance of the point FGT depends on δ , which controls the tree depth and therefore the total number of boxes (and hence the average number of points per leaf box). This dependence can be largely attributed to outgoing to incoming plane wave translations (gather expansions step in [Algorithm 3.2](#)) which requires $O(3^d N_{box} N_F)$ work. This is true for virtually all tree-based algorithms, including FGTs and FMMS. An exception is the one-dimensional FGT based on the sum-of-exponential approximation in [\[12\]](#), which can proceed without a tree data structure, using the ordering of points on the line instead.

As a result, one can get excessively optimistic performance estimates by fixing δ and increasing N alone. A more telling experiment is to reduce δ as we increase N , which we do following the approach used in [\[12\]](#) for two dimensions and in [\[17\]](#) for

three dimensions, where the points are placed on a curve or surface, respectively so that adaptive refinement is necessary. In two dimensions, we fix $N\delta = 400$ and let N vary from 5,000 to 20,000,000. In three dimensions, we use the pairs [17]

$$(\delta = 0.01, N = 10^6), (\delta = 0.007, N = 3.4 \times 10^6), (\delta = 0.005, N = 8 \times 10^6),$$

$$(\delta = 0.004, N = 15.6 \times 10^6), (\delta = 0.003, N = 27 \times 10^6).$$

The corresponding timings are presented in Figure 6.1.

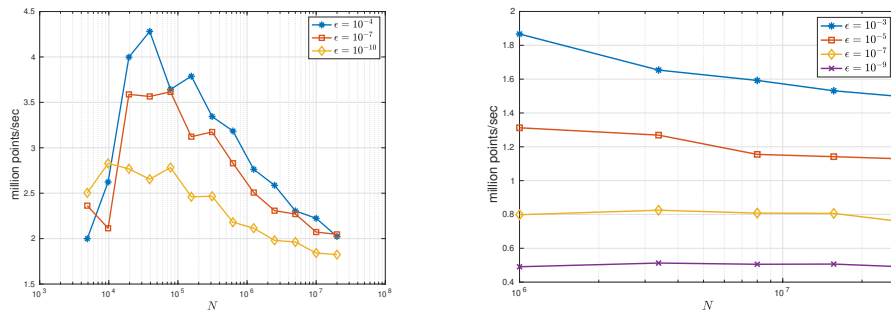


Fig. 6.1: Linear scaling of the point FGT. N here is the total number of points and the y -axis indicates the “throughput” of the FGT measured in units of million points/second. (Left) a 2D problem set up to correspond to Fig. 11 in [12], with points on a curve. (Right) a 3D problem setup to match Tables 4.1-4.4 in [17], with points distributed on a surface.

A second informative experiment is to fix the number of source points and vary δ . For this, we let $N = 10^7$ and let δ range from 10^{-10} to 10^{-1} . We set the target points to be the sources themselves. (Evaluating the field at additional target points comes at very little cost.) In both the two-dimensional and three-dimensional case, we distribute the sources either uniformly in the unit box $B_d \in \mathbb{R}^d$ or uniformly on the surface of the perturbed sphere $S_{d-1} \in \mathbb{R}^d$ (which is highly nonuniform in the ambient space). Timing results are shown in Figure 6.2 and Figure 6.3.

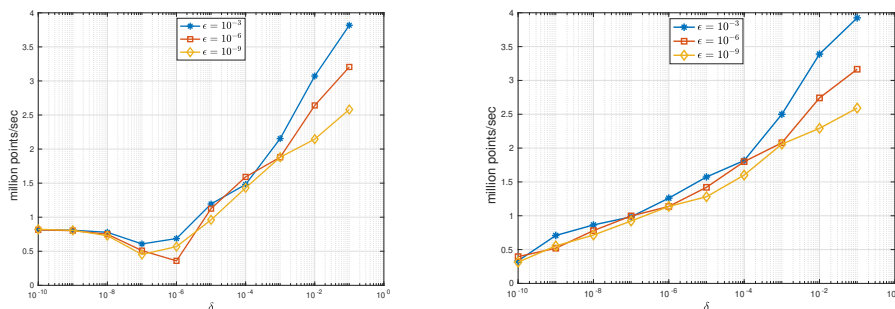


Fig. 6.2: Performance of the 2D point FGT as a function of Gaussian variance, with throughput measured in units of million points per second: (left) a uniform distribution, (right) a highly nonuniform distribution.

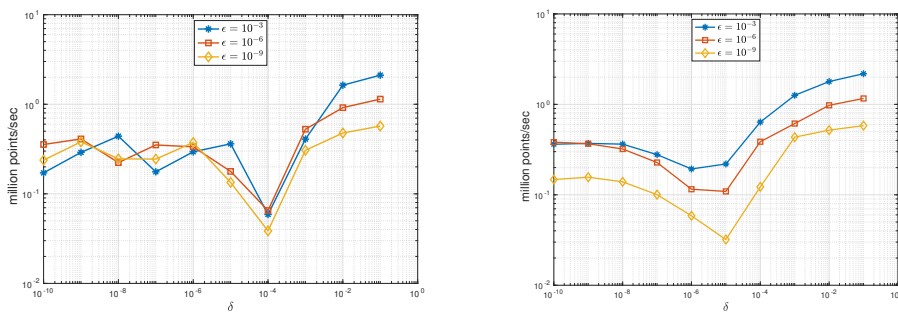


Fig. 6.3: Performance of the 3D point FGT as a function of Gaussian variance, with throughput measured in units of million points per second: (left) a uniform distribution, (right) a highly nonuniform distribution.

REMARK 6.1. *The point FGT can be further accelerated - first by more careful application of the NUFFT (optimizing the FFTW call to make sure it only carries out the “plan” phase once), and second by using special purpose libraries that accelerate the evaluation of exponential functions.*

6.2. Box FGT experiments. We now investigate the performance of the FGT for continuous sources (the “box” FGT). In our experiments, we fix the polynomial approximation order to be $k = 16$, and construct the tree so that the input data is resolved to 10 digits of accuracy on each leaf box. The precomputation of transformation/translation matrices in Algorithm 4.2 takes approximately 1–3 milliseconds, a negligible cost for the problems we consider here.

When considering periodic boundary conditions, we assume the density takes the form

$$(6.1) \quad \sigma_p(\mathbf{x}) = \prod_{\substack{i=1 \\ i \text{ odd}}}^d \sin(2\pi n_p x_i) \prod_{\substack{i=2 \\ i \text{ even}}}^d \cos(2\pi n_p x_i), \quad \mathbf{x} \in \mathbb{R}^d.$$

Refinement in this case leads to a uniform tree (and the analytical expression for the potential is available by Fourier analysis). For our free space examples, we define the density as the sum of several sharply peaked Gaussians

$$(6.2) \quad \sigma_f(\mathbf{x}) = \sum_{i=1}^{n_f} e^{-\|\mathbf{x}-\mathbf{x}_i\|^2/\alpha_i}. \quad \mathbf{x} \in \mathbb{R}^d$$

For $d = 3$, we let

$$(6.3) \quad [\mathbf{x}_1, \dots, \mathbf{x}_5] = [(-0.3, -0.4, -0.06), (-0.2, 0, -0.25), \\ (0.18, -0.1, -0.03), (-0.09, 0.3, 0.17), (-0.38, -0.05, -0.17)],$$

and for $d = 2$, we let \mathbf{x}_i be the projections of the points in (6.3) to the x_1x_2 plane. We specify the corresponding α_i ’s below. The expression for the potential, given the density (6.2), is easily obtained analytically.

We first demonstrate the linear scaling of the box FGT, fixing $\delta = 10^{-3}$. For the periodic box FGT in 2D, we use the density (6.1) with $n_p = 8, 16, 32, 64$. For the free-space box FGT in 3D, we use the density (6.2) and increase the number of Gaussians

n_g from 2 to 5 with $\alpha_1 = 10^{-2}/n_g$ and $\alpha_i = \alpha_1/i$ for $i = 2, 3, 4, 5$. This forces the use of more and more points to resolve the density as n_g increases. Figure 6.4 shows our results, with the throughput measured in million points per second for various precisions.

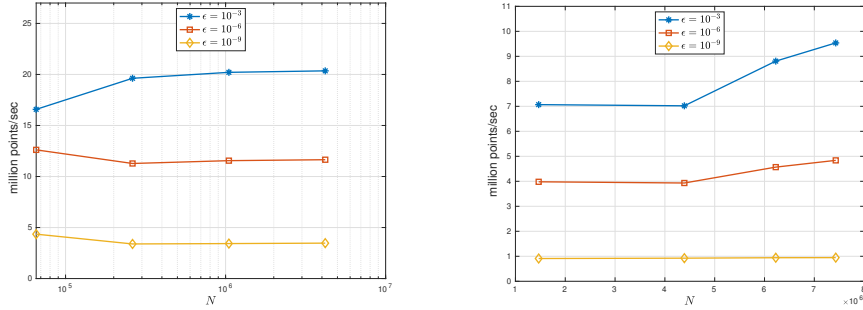


Fig. 6.4: Linear scaling of the box FGT. Here, N is the total number of tensor product grid points in the tree. The y -axis indicates the throughput of the box FGT measured in units of million points/second: (left) a 2D periodic example, (right) a 3D free-space example.

To study the effect of the Gaussian variance δ , we compute the continuous periodic Gauss transform with density given by (6.1), where $n_p = 32$ for $d = 2$ and $n_p = 4$ for $d = 3$. For the free-space case, we use the density (6.2) with $n_g = 5$. We set $\alpha_1 = 10^{-5}$ for $d = 2$ and $\alpha_1 = 4 \cdot 10^{-3}$ for $d = 3$. We set $\alpha_i = \alpha_1/i$ for $i = 2, 3, 4, 5$ for both $d = 2$ and $d = 3$. We then vary δ from 10^{-10} to 1. The timings are shown in Figure 6.5 and Figure 6.6 for $d = 2$ and $d = 3$, respectively. Note that the box FGT becomes very fast for either very small or very large values of δ . In the first case, all interactions are direct and even the 1D transformation matrices $T_{pot \rightarrow pot}$ become sparser and sparser as $\delta \rightarrow 0$. On the other hand, when δ is very large, only a few plane-wave expansions are needed for the entire computational domain.

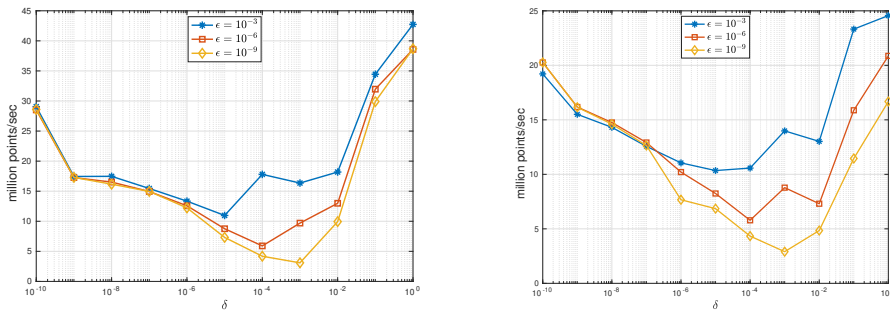


Fig. 6.5: Performance of the 2D box FGT as a function of Gaussian variance: (left) periodic Gauss transform of the density (6.1) with about one million points, (right) free-space Gauss transform of the density (6.2) with about a quarter of a million points.

7. Conclusions and further discussions. We have developed a new version of the fast Gauss transform which combines the benefits of the single-level plane-wave

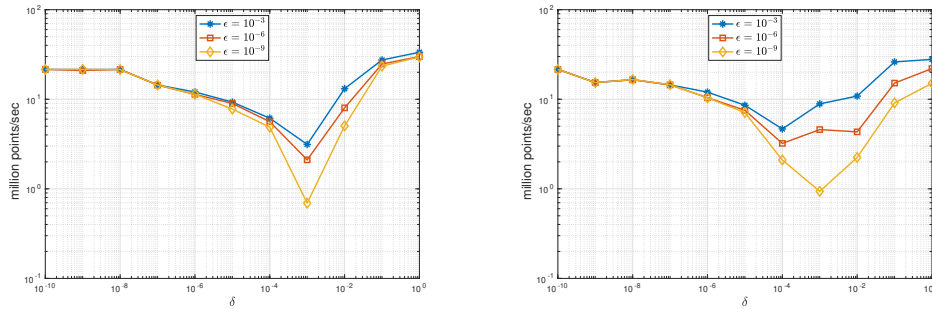


Fig. 6.6: Performance of the 3D box FGT as a function of Gaussian variance: (left) periodic Gauss transform of the density (6.1) with about two million points, (right) free-space Gauss transform of the density (6.2) with about six million points.

based approach of [11, 16, 17] with hierarchical merging, as in [24]. For discrete sources, the scheme refines to a uniform cut-off level, and makes use of the NUFFT to convert the source distribution in a cut-off level box to a plane-wave expansion. For continuous sources, discretized on adaptive tensor product grids, separation of variables allows for the direct mapping of the source density to the plane-wave representation at even greater speeds. We have limited ourselves to dimensions $d \leq 3$ but the algorithm could be pushed a little further although it does not avoid the curse of dimensionality. We did not consider one-dimensional examples in any detail, partly because ordering of the unknowns on the real line permits the use of the SOE (sum-of-exponentials)-based scheme [12]. This is even faster for 1D problems but, as it turns out, not as fast as the present scheme for $d > 1$.

There are a number of computational kernels which can be approximated as a sum of Gaussians (see, for example, [3, 4]) and the FGT described here helps accelerate the corresponding integral transforms. We are currently integrating the new FGT into solvers for time-dependent diffusion problems. We also plan to release an open source software package for the new scheme in the near future.

Finally, we note that the current implementation is not fully optimized for modern CPUs. For example, no use is made of SIMD vectorization in any part of the code, including the FINUFFT library [1]. It is, in fact, possible to remove the dependence on NUFFT entirely, even in the point FGT, by replacing the original source distribution in a leaf node with an equivalent tensor product grid of “proxy points,” as in [15]. Transformation to the plane-wave basis can then be carried out in tensor product form with level-3 BLAS acceleration. Such low-level modifications are likely to increase the throughput of the point FGTs over the data presented in section 6, even though the reduction in terms of operation count is small.

REFERENCES

- [1] A. BARNETT AND J. MAGLAND, *Non-uniform fast Fourier transform library of types 1, 2, 3 in dimensions 1, 2, 3*. <https://github.com/ahbarnett/finufft>, 2018.
- [2] A. H. BARNETT, J. F. MAGLAND, AND L. AF KLINTEBERG, *A parallel non-uniform fast Fourier transform library based on an “exponential of semicircle” kernel*, SIAM J. Sci. Comput., 41 (2019), pp. C479–C504.
- [3] G. BEYLKIN AND L. MONZÓN, *On approximation of functions by exponential sums*, Appl. Comput. Harmon. Anal., 19 (2005), pp. 17–48.

- [4] ———, *Approximation by exponential sums revisited*, Appl. Comput. Harmon. Anal., 28 (2010), pp. 131–149.
- [5] A. DUTT AND V. ROKHLIN, *Fast Fourier transforms for nonequispaced data*, SIMA J. Sci. Comput., 14 (1993), pp. 1368–1393.
- [6] ———, *Fast Fourier transforms for nonequispaced data. II*, Appl. Comput. Harmon. Anal., 2 (1995), pp. 85–100.
- [7] A. ELGAMMAL, R. DURAIWAMI, AND L. S. DAVIS, *Efficient kernel density estimation using the fast Gauss transform with applications to color modeling and tracking*, IEEE Transactions on Pattern Analysis and Machine Intelligence, 25 (2003), pp. 1499–1504.
- [8] L. GREENGARD AND J. LEE, *Accelerating the nonuniform fast Fourier transform*, SIAM Rev., 46 (2004), pp. 443–454.
- [9] L. GREENGARD AND V. ROKHLIN, *A fast algorithm for particle simulations*, J. Comp. Phys., 73 (1987), pp. 325–348.
- [10] L. GREENGARD AND J. STRAIN, *The fast Gauss transform*, SIAM J. Sci. Statist. Comput., 12 (1991), pp. 79–94.
- [11] L. GREENGARD AND X. SUN, *A new version of the fast Gauss transform*, Documenta Mathematica, III, (1998), pp. 575–584.
- [12] S. JIANG AND L. GREENGARD, *Approximating the gaussian as a sum of exponentials and its applications to the fast Gauss transform*, Communications in Computational Physics, 31 (2022), pp. 1–26.
- [13] D. LEE, A. GRAY, AND A. MOORE, *Dual-tree fast Gauss transforms*, Advances in Neural Information Processing Systems, 18 (2006), pp. 747–754.
- [14] F. W. J. OLVER, D. W. LOZIER, R. F. BOISVERT, AND C. W. CLARK, eds., *NIST Handbook of Mathematical Functions*, Cambridge University Press, May 2010.
- [15] R. PEI, T. ASKHAM, L. GREENGARD, AND S. JIANG, *A fast method for imposing periodic boundary conditions on arbitrarily-shaped lattices in two dimensions*, J. Comput. Phys., 474 (2023), p. 111792.
- [16] R. S. SAMPATH, H. SUNDAR, AND S. VEERAPANENI, *Parallel fast Gauss transform*, in SC Proceedings of the ACM/IEEE International Conference for High Performance Computing, Networking, Storage and Analysis, New Orleans, LA, 10 (2010), pp. 1–10.
- [17] M. SPIVAK, S. K. VEERAPANENI, AND L. GREENGARD, *The fast generalized Gauss transform*, SIAM J. Sci. Comput., 32 (2010), pp. 3092–3107.
- [18] J. STRAIN, *Fast adaptive methods for the free-space heat equation*, SIAM J. Sci. Comput., 15 (1994), pp. 185–206.
- [19] H. SUNDAR, R. S. SAMPATH, AND G. BIROS, *Bottom-up construction and 2:1 balance refinement of linear octrees in parallel*, SIAM Journal on Scientific Computing, 30 (2008), pp. 2675–2708.
- [20] J. TAUSCH AND A. WECKIEWICZ, *Multidimensional fast Gauss transforms by Chebyshev expansions*, SIAM J. Sci. Comput., 31 (2009), pp. 3547–3565.
- [21] L. N. TREFETHEN, *Approximation Theory and Approximation Practice*, SIAM, Philadelphia, PA, 2013.
- [22] ———, *Multivariate polynomial approximation in the hypercube*, Proceedings of the American Mathematical Society, 145 (2017), pp. 4837–4844.
- [23] S. K. VEERAPANENI AND G. BIROS, *The Chebyshev fast Gauss and nonuniform fast Fourier transforms and their application to the evaluation of distributed heat potentials*, J. Comput. Phys., (2008). 7768–7790.
- [24] J. WANG AND L. GREENGARD, *An adaptive fast Gauss transform in two dimensions*, SIAM J. Sci. Comput., 40 (2018), pp. A1274–A1300.